metals

MDPI

Article

Synthesizing of Metallized Acrylic Containing Both Gadolinium and Lead as a Transparent Radiation Shielding Material and Its Physical Properties

Bo Zhang [1], Fang Wang [2], Yanke Liu [2], Haoyu Yu [2,*], Yuansong Zeng [2] and Lihui Lang [1,*]

[1] School of Mechanical Engineering and Automation, Beihang University, Beijing 100191, China; zhangbo@avic.com
[2] Department of Material Application Researching, AVIC Manufacturing Technology Institute, Beijing 100024, China; wangf169@avic.com (F.W.); liuyk021@avic.com (Y.L.); yszeng@hotmail.com (Y.Z.)
* Correspondence: yuhy009@avic.com (H.Y.); lang@buaa.edu.cn (L.L.)

Abstract: In this study, a series of optically transparent metallized acrylics containing Gd and Pb were synthesized by the bulk polymerization of $Gd(MAA)_3$, $Pb(MAA)_2$ and AM according to different polymerization procedures. The variation of their optic transmittance and mechanical performance with Gd contents was investigated. Then, quasi-static uniaxial tensile tests under different strain rates and temperatures were performed to study the influence of strain rate and temperature on the mechanical properties of radiation-shielding metallized acrylic containing both Gd and Pb. The tensile responses of this material distinctly exhibit nonlinear characteristics and strongly depend on both temperature and strain rate. Based on the experimental results, a modified Zhu–Wang–Tang (ZWT) constitutive model, in which the standard elastic component was replaced by the Mooney–Rivlin hyperelastic model, was implemented to characterize the observed both hyperelastic and viscoelastic behaviors. The constitutive parameters were expressed as functions of temperature and determined by experimental data. The model fitting results indicate that the selected constitutive model can accurately describe the nonlinear tensile stress–strain responses of metallized acrylic containing Gd and Pb. Furthermore, the great difference in constitutive parameters implies that the viscoelastic behavior of the as-prepared metallized acrylic affects the response to quasi-static tensile loading the most.

Keywords: metallized acrylic; ionizing radiation; gadolinium; ZWT constitutive model; uniaxial tension; temperature dependence; viscoelastic

Citation: Zhang, B.; Wang, F.; Liu, Y.; Yu, H.; Zeng, Y.; Lang, L. Synthesizing of Metallized Acrylic Containing Both Gadolinium and Lead as a Transparent Radiation Shielding Material and Its Physical Properties. *Metals* **2022**, *12*, 990. https://doi.org/10.3390/met12060990

Academic Editor: Ronald W. Armstrong

Received: 30 April 2022
Accepted: 3 June 2022
Published: 10 June 2022

1. Introduction

Gadolinium, which is a rare-earth metal of the lanthanide series, is widely used in nuclear power plants as the control rod for thermal neutron absorption [1,2] because its two isotopes Gd 155 [3] and Gd 157 [4] possess the largest neutron-capture cross-sections among all the natural isotopes of any element. Therefore, gadolinium is considered the best radiation shielding element. Based on that fact, Gd and its chemical compounds are essential components of radiation shielding silicate glass for the observation windows in nuclear power plants or the radiology examination rooms of hospitals [5,6], where ionizing radiation such as neutron radiation and X-ray is spreading in the environment. However, when neutrons are absorbed by Gd atoms, it excites secondary gamma rays [7], although the hazards of radiating energy are significantly reduced. Hence, lead is commonly used as a co-shielding element with Gd because of its excellent absorbing capacity for gamma ray [8]. Regrettably, the mechanical performance of inorganic transparent radiation-shielding materials such as Gd and Pb silicate glass is unsatisfied because of their high fragility and undesirable formability.

By contrast, optically transparent organic materials, especially the polymeric materials, such as acrylics and polycarbonates are of lower density and brittleness, and they could be formed into complex shapes. The metallized derivatives of those polymers containing Gd and Pb could combine the shielding properties of those two metals with the mechanical performance of the organics. There are great expectations for consequent metallized polymers to replace inorganic shielding materials in medical, atomic energy, military and many other industrial sectors [9,10]. Thus, significant investment was made into the fabrication of those transparent metallized organic materials. Lin et al. [11] prepared radiation-shielding polymer according to the ternary copolymerization of lead methacrylate, styrene and methacrylic acid, which possess good optical properties. Chen et al. [12] synthesized acrylic glass containing Pb by means of microemulsion polymerization. This material exhibits better physical performance than those synthesized by bulk polymerization. However, compared with ordinary acrylics, its mechanical properties are significantly degraded. For instance, the impact strength of this Pb-containing acrylic is only 3 KJ/m^2. Therefore, to fabricate a new metallized polymeric material with excellent mechanical performance is of great significance to promote the practical use of this kind of material. Aiming to ameliorate both mechanical performance and radiation-shielding property, our research group improved the reaction ingredients and successfully prepared a metallized acrylic containing both Gd and Pb, and the impact strength of the metallized acrylic was greater than 20 KJ/m^2.

Equally important, establishing an accurate constitutive model for this radiation-shielding material is quite essential for understanding its usability and formability. Presently, the Zhu–Wang–Tang (ZWT) [13–17] nonlinear viscoelastic constitutive model is a well-accepted representation for describing the mechanical properties of various materials under different strain rates. This model has shown its validity in modelling the rate-dependent nonlinear viscoelastic behavior of numerous materials such as polymethyl methacrylate (PMMA) [18,19], concrete [20], soil [21], etc. Especially, the polymeric materials under a strain rate range between 10^{-4} s^{-1} and 10^{3} s^{-1} can be well described by the ZWT constitutive model within the deformation limit [22]. Regrettably, the typical ZWT model can only describe the mechanical properties within a deformation limit of 8% [23] and not suit the materials that exhibit hyperelastic behaviors. Nevertheless, this model require too many parameters which are not suitable for engineering applications [24]. Therefore, Jiang et al. [25] developed an improved ZWT nonlinear visco-hyperelastic constitutive model, in which a Mooney–Rivlin hyperelastic model is introduced to replace the nonlinear elastic equilibrium response element for effectively modeling the complex behaviors of polymeric materials under quasi-static and dynamic loadings. Considering the hyperelastic behavior observed during the uniaxial tension tests of metallized acrylic containing Gd and Pb, the modified ZWT constitutive model is more reliable to describe both hyperelastic and viscoelastic properties of this material simultaneously.

In this study, a kind of transparent metallized acrylic containing both Gd and Pb was successfully synthesized by the bulk polymerization of organometallic acrylic monomers. This radiation-shielding metallized acrylic exhibits good optical transparency and acceptable thermal stability. Furthermore, this study investigates the mechanical properties of metallized acrylic containing Gd and Pb. Quasi-static uniaxial tension experiments were performed to study the influence of strain rate. Because the metallized acrylic has both hyperelasticity and viscoelasticity responses to tensile loadings, the modified ZWT model was then conducted to describe the behavior of this material. After that, this model was employed to research the stress–strain behavior at different temperature by fitting the constitutive parameters to the experimental data. Subsequently, the tendency of those parameters was expressed as functions of temperature and determined by interpolation fitting. The fitting results were further researched with the aim of confirming the main factor that affects the response of metallized acrylic containing Gd and Pb.

2. Materials and Methods

2.1. Chemicals and Materials

All reagents and solvents were of at least analytical grade and purchased from commercial suppliers. Gadolinium oxide (Gd_2O_3) was purchased from Shandong Liang Zheng New Material Technology Co., Ltd. (Zibo, Shandong, China). Diethyl-bisphenol A dimethacrylate ($BPA(EO)_2DA$), lead oxide (PbO), azodiisobutyronitrile (AIBN), acrylamide (AM), ethanol, and octanoic acid (OA) were obtained from Sinopharm Chemical Reagent Co., Ltd. (Beijing, China). MMA was washed by sodium hydroxide solution and distilled water to eliminate the inhibitors. AIBN was recrystallized before use. Gadolinium methacrylate ($Gd(MAA)_3$) and lead methacrylate ($Pb(MAA)_2$) were prepared by the method mentioned in the reference [26].

2.2. Preparation of Metallized Acrylic Containing Gd and Pb

Desired amounts of $Gd(MAA)_3$, $Pb(MAA)_2$, AM, $BPA(EO)_2DA$ and OA were added into a 10 L reactor and stirred at 75 °C for at least 20 min until all powder was dissolved. The consequent solution was pre-polymerized with the initiation of AIBN under continuous stirring for 15 min. The prepolymer was then poured into a planar mold made of two pieces of tempered silica glass, and it was cured according to a designed polymerization procedure which contained a series of periods under different temperatures. Finally, the metallized acrylic sheet containing both Gd and Pb was obtained after removal of the mold.

2.3. Characterizations and Shielding Performance Analysis

Light transmittance was measured on a 722 visible spectrophotometer (Shanghai Jinghua Technology Instrument Co., Ltd., Shanghai, China) at the wavelength of 550 nm. Fourier transform infrared (FTIR) spectroscopy was conducted using a Thermo Nicolet IS 50 spectrometer (Thermo Fisher Scientific (China) Co., Ltd., Shanghai, China). The ultraviolet-visible (UV-Vis) spectra were obtained by a PerkinElmer Lambda 1050+ UV/Vis Spectrophotometer (Perkinelmer Management (Shanghai) Co., Ltd., Shanghai, China) in the range of 200–800 nm.

The shielding performance were measured on a TW32002 spherical ionization chamber (PTW Freiburg GmbH., Freiburg, Germany), the energy selected for neutron-shielding performance is 0.025 eV, and the energy selected for X-ray shielding performance is 100 keV.

2.4. Mechanical Properties Tests

The specimens for unnotched impact, bending and uniaxial test were obtained by machining the metallized acrylic containing Gd and Pb, according to the standards ISO 180:2000, ISO 178:2001, and DIN EN ISO 527-1:2012, respectively. The CNC lath we used was a FEELER VMP-23A (Fair Friend Ent. Co., Ltd., Taipei, Taiwan, China) in the factory of Beijing Hangda Yijie Technology Co., Ltd. Particularly, the uniaxial tension test was firstly conducted on a ZWICK Z020 universal testing machine (ZwickRoell Testing Systems Co., Ltd., Taicang, China) with three strain rates of 2 mm/min, 5 mm/min and 10 mm/min under 100 °C to investigate the mechanical properties of the metallized acrylic containing Gd and Pb and to characterize the strain rate dependence of this material. The corresponding tensile strain rates were 6.67×10^{-4} s^{-1}, 1.67×10^{-3} s^{-1}, and 3.33×10^{-3} s^{-1}, respectively. Then, the stress–strain response to temperature was tested under 60 °C, 80 °C, 90 °C, 95 °C, and 100 °C at the strain rate of 1.67×10^{-4} s^{-1}. The nominal stress and strain data are converted into true stress and true strain data by using incompressibility assumption. The impact strength test was conducted on a MZ-2056B digital impact testing machine (Jiangsu Mingzhu Testing Co., Ltd., Yangzhou, China).

3. Results and Discussion

3.1. The Properties of Metallized Acrylic under Different Formulations

The metallized acrylic prepared according to different formulations were first made into 4 mm thickness sheets, in which the content of $Pb(MAA)_2$ was 30% and the content of

$Gd(MAA)_3$ was 5%. Although $Gd(MAA)_3$ and $Pb(MAA)_2$ are solid powders, they show excellent dispersion in other monomers selected in the formulas. The basic performance of metallized acrylic is shown in Table 1. As can be seen from the results, the bending strength of the material gradually increases with the rising level of AM content. Commonly, the addition of polar monomers, such as AM, would form more hydrogen bonds, which will strengthen the cohesive force between polymeric molecules and additionally improve the mechanical performance of the bulk material. However, both AM and organometallic monomers are solid state; excessive charge will cause incomplete dissolution. Thus, the amount of AM cannot continually increase. $BPA(EO)_2DA$ has a high optical refractive index of 1.542, which is good for improving the light transmittance of the material. That is why when the content of the $BPA(EO)_2DA$ monomer decreases, the light transmittance decreases, too. By comparing the overall properties of the materials, when the ratio of $BPA(EO)_2DA$/AM/MAA is 20/27.5/2.5, the metallized acrylic obtains the best mechanical performance, of which the impact strength and bending strength reaches 21.91 KJ/m^2 and 93.45 MPa, respectively. Meanwhile, the light transmittance under this formulation is adequate.

Table 1. The properties of metallized acrylic containing both Gd and Pb.

Sample Code	$BPA(EO)_2DA$ /AM/MAA	Transmittance/%	Impact Strength/KJ/m^2	Bending Strength/MPa
A-1	25/20/5	89.2	20.43	60.97
A-2	25/22.5/2.5	89.1	17.86	78.21
A-3	20/25/5	87.6	13.46	89.32
A-4	20/27.5/2.5	87.0	21.91	93.45

3.2. Polymerization Results of the Metallized Acrylic under Different Polymerization Procedure

In order to obtain adequate shielding performance, the metallized acrylic should have a certain thickness. Thus, on the basis of the previous formula, a 12 mm thick plate polymerization process was studied. The bulk polymerization of metallized acrylic is divided into three stages, which successively are prepolymerization, low-temperature polymerization and high-temperature post-treatment. Commonly, the polymeric reactions of acrylate monomers are accompanied by volume contraction. In order to reduce the volume shrinkage effect, prepolymerization should be carried out first. When the polymeric system attains a certain viscosity, the resulting solution is poured into the planar mold to proceed the low-temperature polymerization. In this stage, considerable heat is generated as the reaction is exothermic. Consequently, the reacting system will implode if the excess heat is not timely removed from the solution, which possess poor thermal conductivity. Based on that fact, water, which has a high specific thermal capacity, was selected as the heating medium for this low-temperature polymerization stage. Afterwards, the high-temperature polymerization proceeded in an oven, because the heat release is weak at this stage. Table 2 presents the comparation of optical and mechanical properties of metallized acrylic prepared by different polymerization procedures. Those procedures were composed of several polymerization stages under different temperatures and reaction times. It can be seen that the sample B-1 has the minimum impact and bending strength among the resultant polymers of the three polymerization procedures. That result could be explained as the polymerization proceeding too long under a relatively low temperature of 55 °C, which led to an excessive consumption of initiator. The remaining initiator could not promote the extent of reaction at the high temperature stage and reduce the polymerization degree of the consequent acrylic. Compared with B-2, B-3 increases the heating program of 80 °C and prolongs the reaction time; it further improves the bending strength according to the increase of the reaction degree. Through a comprehensive performance comparison of materials, the polymerization procedure is determined as 55 °C/12 h + 60 °C/4 h + 80 °C/2 h + 100 °C/2 h for the preparation of a 12 mm thick plate. The material has better mechanical properties compared to other brittle radiation shielding metallized acrylics [12].

Table 2. The properties of metallized acrylic containing both Gd and Pb.

Sample Code	Polymerization Procedure	Transmittance/%	Impact Strength/KJ/m^2	Bending Strength/MPa
B-1	55 °C/22 h + 60 °C/4 h + 100 °C/2 h	76.3	22.33	55.46
B-2	55 °C/12 h + 60 °C/4 h + 100 °C/2 h	79.9	30.46	82.59
B-3	55 °C/12 h + 60 °C/4 h + 80 °C/2 h + 100 °C/2 h	80.9	28.34	101.36

3.3. Infrared Spectrogram of Metallized Acrylic Containing Gd and Pb

The preparation of metallized acrylic undergoes a reaction process of free radical polymerization. That is mainly the addition reaction of carbon double bonds of monomers with propagating chain radicals. During the polymerization period, the C=C double bond is gradually consumed and turns into a C–C chain. All chemical changes can be detected by the variation in infrared response. Figure 1 shows the FTIR spectrum of metallized acrylic. It can be seen that the peaks at 2925 cm^{-1} and 2854 cm^{-1} belong to the stretching vibration of the C–H bond of –CH_3 and –CH_2 group. The diffuse peak covers the wavelength range from 3700 to 3030 cm^{-1} and can be assigned to the –NH_2 and –COOH groups of AM and MAA units in the polymer chain. The broadened peak width indicates the existence of intermolecular hydrogen bonds. The stretching vibration peak of the C=C double bond at 1710 cm^{-1} in the metallized acrylic containing both Gd and Pb basically disappeared. This phenomena has proved that Gd and Pb elements are chemically bonded into the acrylic copolymers by the co-polymerization of Gd $(MAA)_3$, $Pb(MAA)_2$ and other monomers [27].

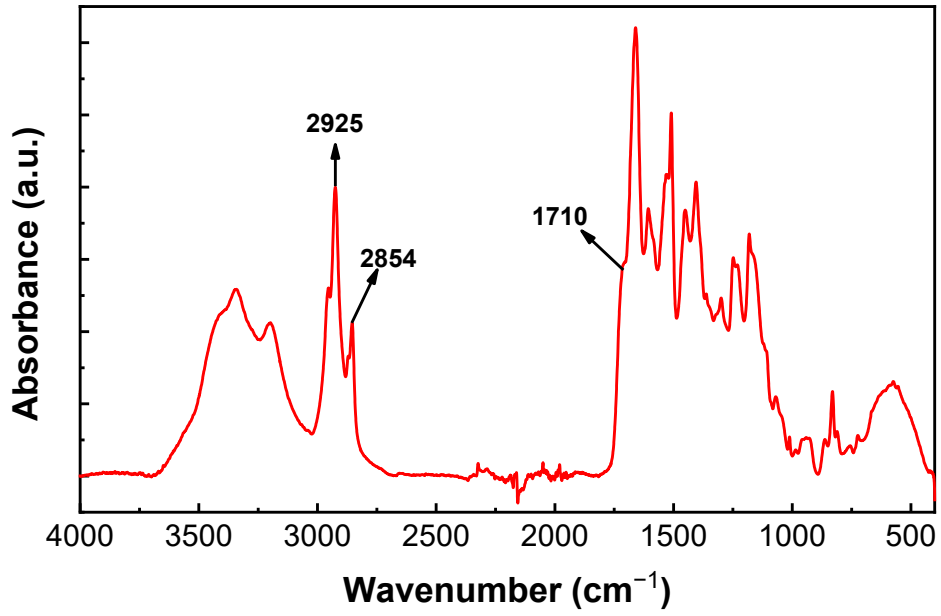

Figure 1. The FTIR spectrum of metallized acrylic.

3.4. The Variation of Transmittance of Metallized Acrylic with Contents of Gd

A transparent material should possess a desirable optical transmittance. Figure 2 shows the transmittance of metallized acrylic with different $Gd(MAA)_3$ content; the thickness of metallized acrylic is 12 mm, and it was prepared by the polymerization process mentioned above. Obviously, with the increase in $Gd(MAA)_3$ content, the transmittance of the metallized acrylic decreases gradually. This phenomenon is due to the dispersity of $Gd(MAA)_3$ oligomer decrease with the raising of $Gd(MAA)_3$ monomer concentration, resulting in the discontinuity or irregular enhancement of optical property form the internal to the surface of the material [28]. In detail, because the $Gd(MAA)_3$ has higher polymerization activity than other monomers, according to the kinetics of polymerization [26], this metallized monomer is more likely to self-polymerize while the concentration rises up.

Consequently, the $Gd(MAA)_3$ oligomer, which has higher molecular wight and density, precipitates to the bottom to the flatwise set flat mold [29]. Therefore, the fluctuation of molecular density in the material leads to the fluctuation of refractive index, which enhances the scattering of light through the material macroscopically and leads to the decrease in transmittance. When the content of $Gd(MAA)_3$ is less than 7%, the transmittance of the glass is greater than 80%, so in practical application, the content of $Gd(MAA)_3$ should be less than 7%.

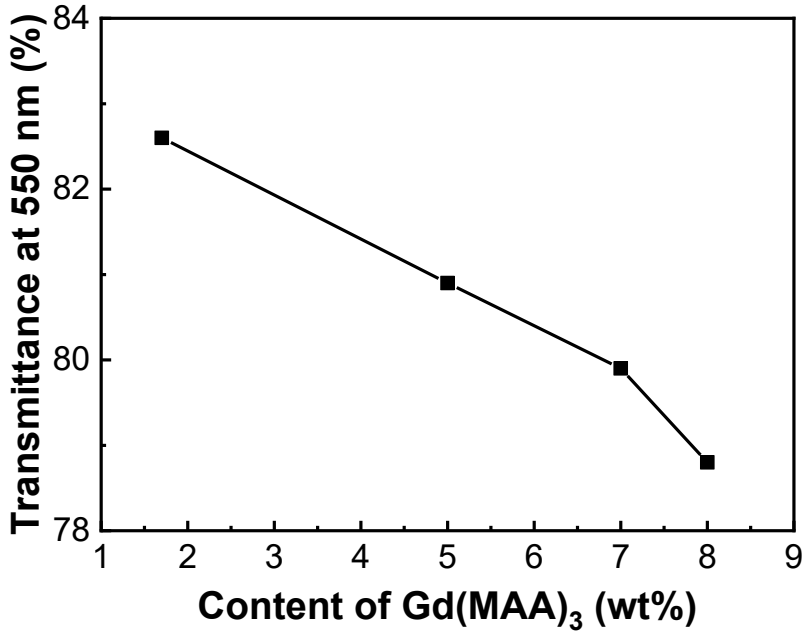

Figure 2. The transmittance of metallized acrylic with different $Gd(MAA)_3$ content.

3.5. The Mechanical Property of Metallized Acrylic Containing Both Gd and Pb

Based on the basic prescription of monomers, the content of $Pb(MAA)_2$ was fixed. Therefore, the concentration of Pb became a control variable in the study of the effects of metal element Gd on the mechanical properties of acrylic. It can be seen from Figure 3 that the bending strength was increased with the elevating content of $Gd(MAA)_3$, and the impact strength went the other way. It is because the organometallic monomer contains multiple double bonds, resulting in a crosslinked as-prepared copolymer. This thermoset copolymer constructs a three-dimensional network, which strengthens the bulk material as the polymerization goes on. The greater the content of $Gd(MAA)_3$, the greater the degree of crosslinking. Moreover, the enlarging molecular weight also contributes to the increasing of bending strength. However, whereas the strong polarity of $Gd(MAA)_3$ increases the intermolecular force, the large side groups make the main chain of the as-polymerized acrylic difficult to adjust conformation by asymmetrical rotation. The steric effect restrains the mobility of the molecular chain and thereby reduces impact strength [30].

3.6. The Shielding Performance of Metallized Acrylic Containing Both Gd and Pb

The metallized acrylic containing both Gd and Pb possesses the X-ray and neutron proof ability. The neutron protection function is mainly achieved by the Gd atoms. Meanwhile, the X-ray protection function is gained form Pb. The higher the content of the metal elements, the better its shielding performance. Through the above research on the optical and mechanical properties of this material, the content of $Gd(MAA)_3$ was determined to be 5 wt % and the content of $Pb(MAA)_2$ was determined to be 30%. Furthermore, the radiation shielding properties of materials are also affected by thickness. Figure 4 shows the shielding properties of metallized acrylic with different thicknesses. It can be seen that with the increase in thickness, the shielding performance of the material is gradually enhanced. When the thickness reaches 12 mm, the shielding rate for neutrons is 93.6%,

and the shielding efficiency for X-rays is 0.47 mmPb. When the metal element content is constant, increasing the thickness of the metallized acrylic can also obtain excellent radiation shielding performance.

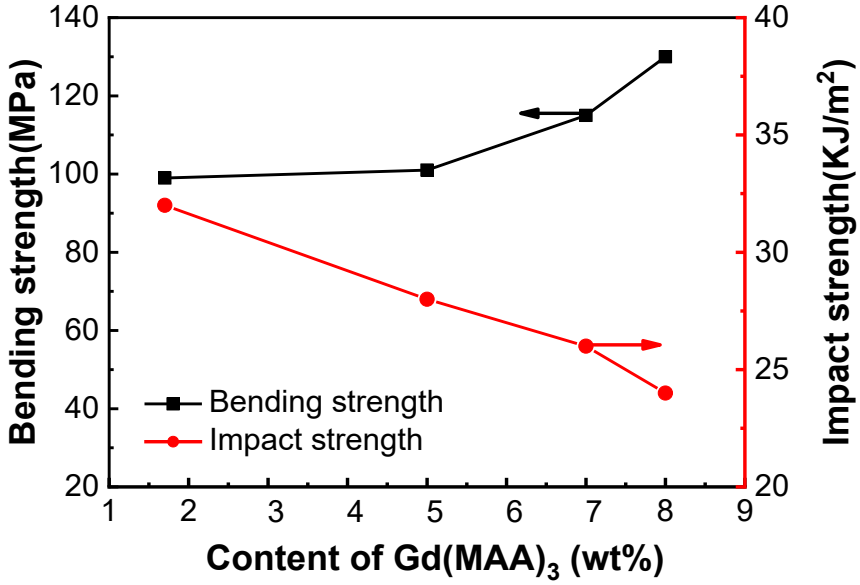

Figure 3. The bending strength and impact strength of metallized acrylic with different $Gd(MAA)_3$ content.

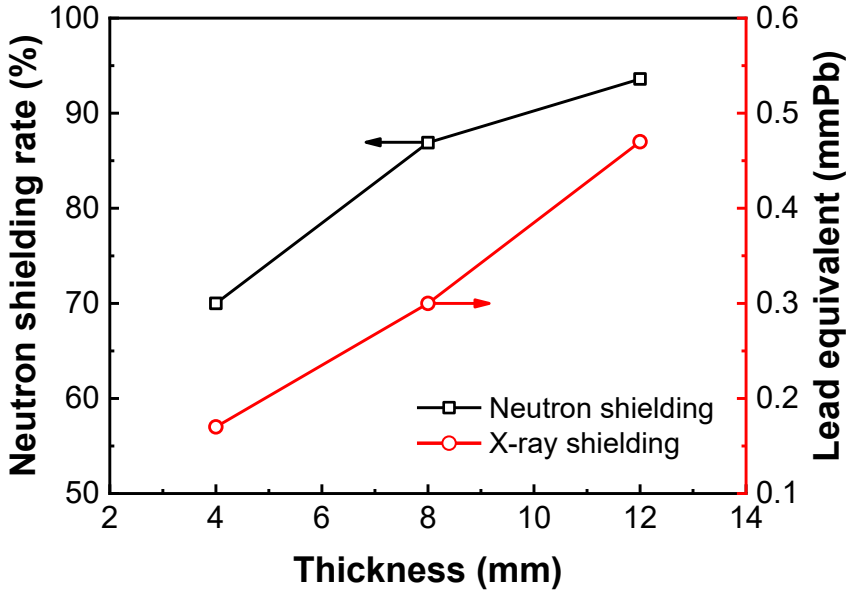

Figure 4. The radiation shielding properties of the metalized acrylic polymerized evaluated by lead equivalent thickness.

3.7. Quasi-Static Uniaxial Tensile Test Results and Model Fitting

3.7.1. The Modified ZWT Constitutive Model

The complex nonlinear viscoelastic behavior of the polymeric materials under a strain rate range between 10^{-4} s^{-1} and 10^{3} s^{-1} can be well described by the ZWT constitutive model within the deformation limit [22]. However, considering the hyperelastic behavior observed during the uniaxial tension tests of organic glass containing Gd and Pb, the modified ZWT constitutive model, in which Mooney–Rivlin hyperelastic model is introduced to replace the nonlinear elastic equilibrium response element, is more reliable to describe both the hyperelastic and viscoelastic properties simultaneously.

- ZWT nonlinear viscoelastic constitutive model

The ZWT constitutive model has shown its validity in modeling the rate dependent nonlinear viscoelastic behavior of numerous materials. The equation of the ZWT constitutive model [31] can be expressed as:

$$\sigma = E_0\varepsilon + a\varepsilon^2 + \beta\varepsilon^3 + E_1\int_0^t \dot{\varepsilon}(\tau)exp\left(-\frac{t-\tau}{\theta_1}\right)d\tau + E_2\int_0^t \dot{\varepsilon}(\tau)\exp\left(-\frac{t-\tau}{\theta_2}\right)d\tau \quad (1)$$

where σ and ε are the true stress and true strain, respectively. E_0, α and β are the parameters describing the nonlinear elastic response. The first and second integration terms describe the viscoelastic response under low and high strain rates, respectively. E_1 and θ_1 are the elastic constant and relaxation time constant of the first Maxwell viscoelastic response. E_2 and θ_2 are the elastic constant and relaxation time constant of the second Maxwell viscoelastic response, and $\dot{\varepsilon}$ is the strain rate.

Under conditions of quasi-static tension, the high-frequency Maxwell element relaxes at the beginning of loading, such that the high strain rate integral term can be neglected, and Equation (1) reduces to

$$\sigma = E_0\varepsilon + \alpha\varepsilon^2 + \beta\varepsilon^3 + E_1\int_0^t \dot{\varepsilon}(\tau)exp\left(-\frac{t-\tau}{\theta_1}\right)d\tau \quad (2)$$

Assuming that the strain rate keeps constant ($\dot{\varepsilon} = const$, $\varepsilon = \dot{\varepsilon}t$), therefore, Equation (2) can be reformed as

$$\sigma = E_0\varepsilon + \alpha\varepsilon^2 + \beta\varepsilon^3 + E_1\theta_1\dot{\varepsilon}\left[1 - exp\left(-\frac{\varepsilon}{\theta_1\dot{\varepsilon}}\right)\right] \quad (3)$$

- Mooney–Rivlin hyperelastic model

Generally, hyperelastic models demonstrate the disproportion between stress and strain under the strain levels that exceed the simple Hookean spring condition. The constitutive models for rubber-like materials have been proposed based on a phenomenological approach or on the intricacies of the micromechanics [32–34]. The Mooney–Rivlin hyperelastic model is widely used by many theoretical investigators and analysts to solve the large elastic deformations of rubber-like materials [35–37].

With the assumption that the as-prepared organic glass is incompressible and isotropic, the hyperelastic constitutive model under one-dimensional stress based on uniaxial loading conditions and the Mooney–Rivlin strain energy function (W) [38] is given as follows:

$$W = C_{10}(I_1 - 3) + C_{01}(I_2 - 3) \quad (4)$$

where C_{10}, C_{01} are empirically determined material parameters, and I_1, I_2 are the principal strain invariants.

With the assumption of full incompressibility (i.e., $\lambda_1 = \lambda$, $\lambda_2 = \lambda_3 = \lambda\hat{}(-1/2)$, where λ_i is the stretch ratio in the i-th direction and λ is the principal stretch ratio), the constitutive relation for uniaxial tension becomes

$$\sigma_T = 2C_{10}\left(\lambda^2 - \frac{1}{\lambda}\right) + 2C_{01}\left(\lambda - \frac{1}{\lambda^2}\right) \quad (5)$$

where σ_T is the true stress of uniaxial tension.

- Modified ZWT constitutive model for organic glass containing Gd and Pb

Aiming to describe both hyperelasticity and viscoelasticity behavior under quasi-static tension of the organic glass containing Gd and Pb at the same time, the elastic equilibrium response element in the simplified ZWT model Equation (3) was replaced by the Mooney–

Rivlin hyperelastic model Equation (5) according to Jiang's research to build the following new constitutive model:

$$\sigma = 2C_{10}\left(\lambda^2 - \frac{1}{\lambda}\right) + 2C_{01}\left(\lambda - \frac{1}{\lambda^2}\right) + E_1\theta_1\dot{\varepsilon}\left[1 - exp\left(-\frac{\varepsilon}{\theta_1\dot{\varepsilon}}\right)\right] \quad (6)$$

Because $\lambda = 1 - \varepsilon$, the mechanical behavior of organic glass containing Gd and Pb under different strain rate loading will be represented by

$$\sigma = 2C_{10}\left((1-\varepsilon)^2 - \frac{1}{(1-\varepsilon)}\right) + 2C_{01}\left((1-\varepsilon) - \frac{1}{(1-\varepsilon)^2}\right) + E_1\theta_1\dot{\varepsilon}\left[1 - exp\left(-\frac{\varepsilon}{\theta_1\dot{\varepsilon}}\right)\right] \quad (7)$$

3.7.2. Tension Responses of Metallized Acrylic Containing Gd and Pb

The uniaxial tensile test results and relevant modified ZWT model fitted curves of the as-prepared metallized acrylic under the strain rates of 6.67×10^{-4} s^{-1}, 1.67×10^{-3} s^{-1}, and 3.33×10^{-3} s^{-1} are shown in Figure 5 (the contents of $Gd(MAA)_3$ and $Pb(MAA)_2$ are 5 wt % and 30%, respectively). It is conspicuous that the mechanical responses of this material exhibit nonlinear behavior and are sensitive to strain rate, and the elastic modulus obviously increases with the increasing of strain rate. Notably, the stress continuously raises with the increasing tensile strain until the specimen breaks at a relatively large deformation scale, and no distinct yielding point and strain softening stage can be observed. However, the stress–strain curves do bend at a certain strain that proves the existence of yielding behavior. The slope of the quasi-linear stage before yield gradually raises up with the increasing of strain rate. All the phenomena indicate that the metallized acrylic containing Gd and Pb has a hyperelastic response and demonstrates a strain-rate dependence. Therefore, we conducted the modified ZWT model to describe the complex mechanical behavior of this material by fitting the constitutive equation to the tensile test results. The fitted curves for each strain rate were generated using Origin software, and they match well with the experimental data. The fitting results show satisfactory accuracy, indicating that the modified ZWT constitutive model is valid for describing the tension responses of metallized acrylic containing Gd and Pb.

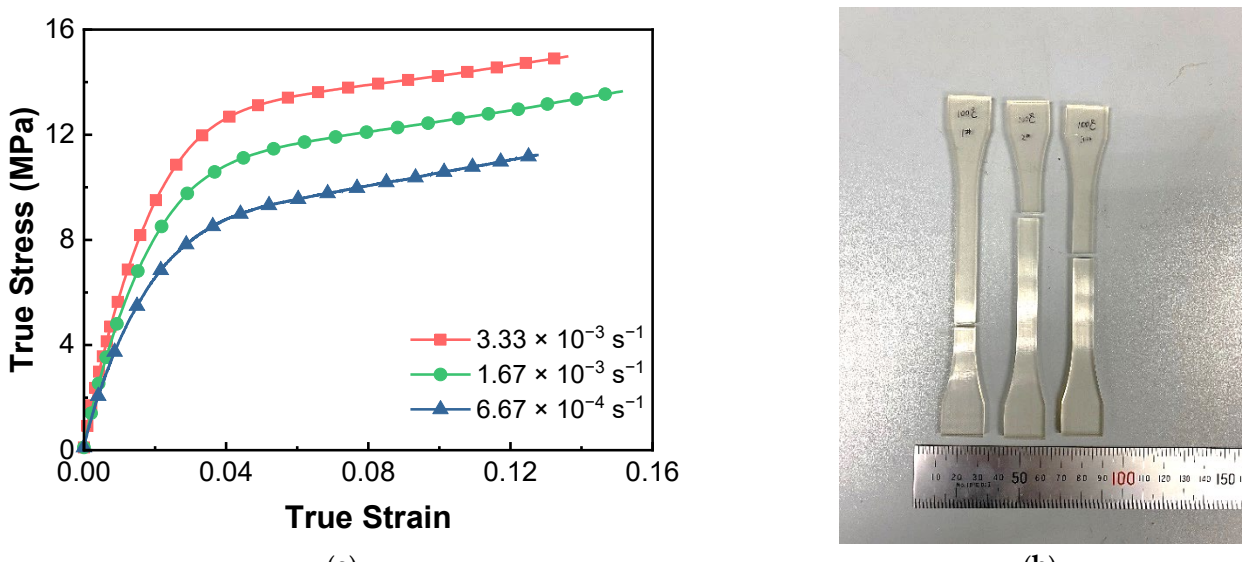

Figure 5. The uniaxial tensile test results of the metallized acrylic containing 5 wt % $Gd(MAA)_3$ and 30 wt % $Pb(MAA)_2$ at 100 °C. (**a**) The true stress–strain curves under different strain rates. (**b**) The fractured metallized acrylic specimens after tensile test at 100 °C.

According to the modified ZWT equation, the third element of $E_1\theta_1\dot{\varepsilon}\left[1-exp\left(-\frac{\varepsilon}{\theta_1\dot{\varepsilon}}\right)\right]$ is obviously affected by the strain rate $\dot{\varepsilon}$ in a positive correlation. Thus, the slope of the fitted curves becomes strain rate dependent.

3.7.3. Temperature Dependence of the Constitutive Parameters of Modified ZWT Model for the Metallized Acrylic

Although the modified ZWT constitutive model has effectively described the rate-dependent nonlinear viscoelastic behavior of the metallized acrylic containing Gd and Pb, the temperature effect, however, is not included in this model. In fact, the experimental tests indicate that the influence of environmental temperature on the mechanical behavior cannot be neglected. Figure 6 shows the stress–strain relations of metallized acrylic with the identical Gd and Pb contents to Figure 5 at 60 °C, 80 °C, 90 °C, 95 °C and 100 °C under the same strain rate of 1.667×10^{-4} s^{-1}. As presented in Figure 5, the uniaxial tension stress shifts dramatically with temperature. It can be seen from Figure 6 that with the elevating temperature level, the slope of the elastic stage declines significantly, implying the reduction in elastic modulus.

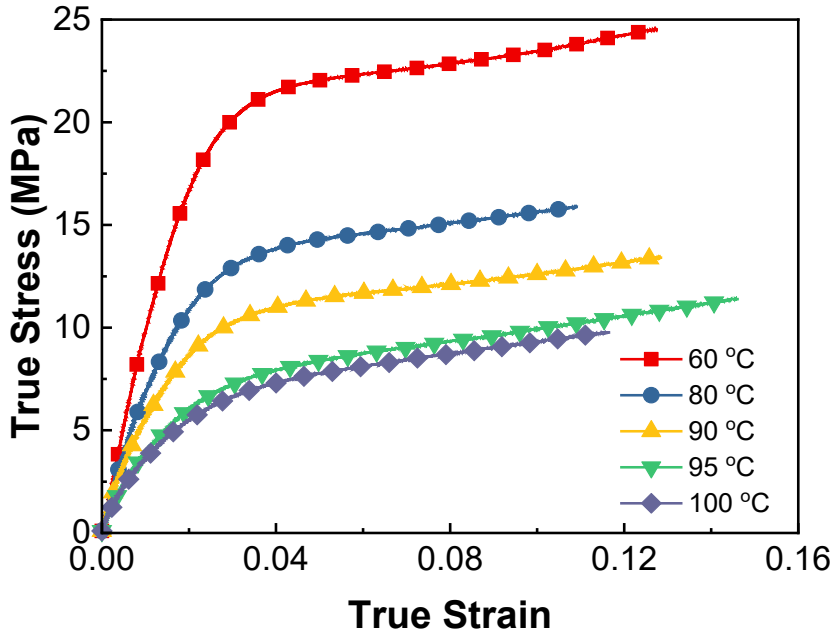

Figure 6. Stress–strain curve of Gb/Pb acrylic under different temperature at the same extension rate of 1.667×10^{-4} s^{-1}.

The parameters of the modified ZWT constitutive model are determined at the temperatures from 60 to 100 °C, as presented in Table 3. Obviously, C_{10}, C_{01}, and E_1 vary gradually with temperature. To describe the stress–strain responses considering the effects of temperature dependence, those model parameters are expressed as functions of temperature. The three functions are determined by cubic and line polynomial interpolating. The interpolation curves and the parameters determined by experimental data are shown in Figure 7a–c. The dimensionless expressions of the interpolation functions are presented in Table 4 with coefficient of determination. It can be observed that the interpolation functions can accurately fit the parameters with temperature variation. When C_{10} rises up with temperature, C_{01} exhibits an opposite tendency. Additionally, E_1 decreases with temperature remarkably, which makes the Maxwell viscoelastic element of the modified ZWT constitutive model play the decisive role in affecting the material's responses to loadings. In addition, θ_1 is seemingly not affected by temperature, suggesting that θ_1 might be only a function of strain rate.

Table 3. Values of the parameters in modified ZWT model at environmental temperature from 60 to 100 °C.

T (°C)	C_{10} (MPa)	C_{01} (MPa)	E_1 (MPa)	θ_1 (s)
60	47.46	−42.95	1689.83	82.74
80	35.27	−32.72	1051.50	85.50
90	22.80	−21.91	819.35	85.50
95	3.34	−6.68	532.99	84.14
100	−8.36	3.10	476.94	79.98

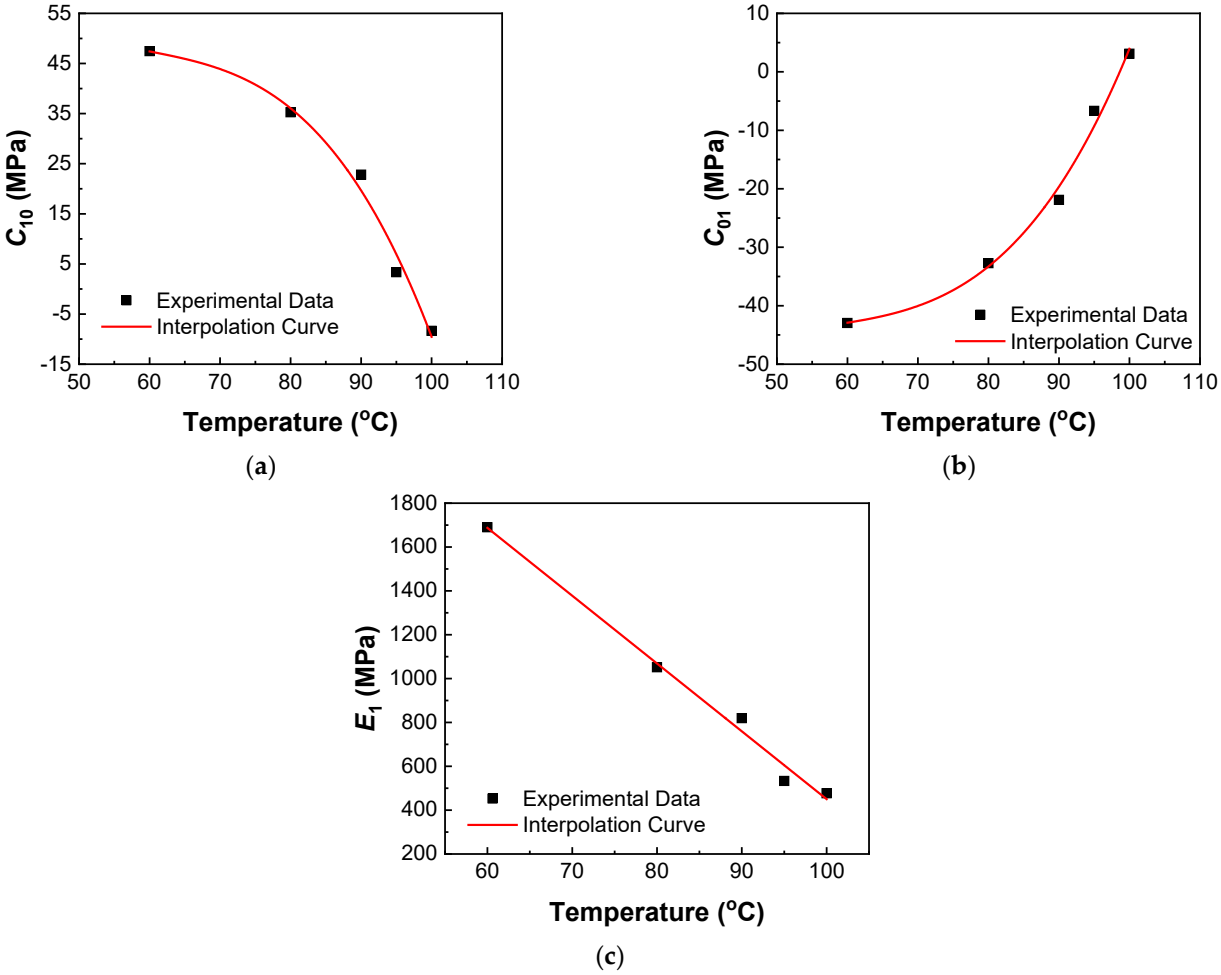

Figure 7. The model parameters' variations with temperature and the interpolation curves: (**a**) C_{10}; (**b**) C_{01}; (**c**) E_1.

Table 4. Interpolation functions of the parameters in modified ZWT model.

Expressions of the Interpolation Functions	R^2
$C_{10} = -7.0722 \times 10^{-4}\ T^3 + 0.1269\ T^2 - 7.8710\ T + 215.4718$	0.9881
$C_{01} = 5.0550 \times 10^{-4}\ T^3 - 0.0868\ T^2 + 5.151\ T - 148.7003$	0.9908
$E_1 = -30.9225\ T + 3542.5324$	0.9899

Based on the interpolation functions of the constitutive parameters, E_1 possesses the maximum absolute-value coefficient of temperature, which means the apparent modulus will significantly decrease with temperature. As a consequence, the fitted ZWT curve strongly depends on temperature in a negative relationship.

4. Conclusions

In this paper, the optimized polymerization procedure of acrylic containing Gd and Pb was selected by the comparison of the optical and mechanical performance of the products. The test results indicated that excess initiator consumption under relatively low reaction temperature will lead to weakness in impact and bending strength. In addition, with the increase in $Gd(MAA)_3$ content, the optic transmittance at 550 nm wavelength decreases gradually, which is due to the inhomogeneous dispersion of $Gd(MAA)_3$ monomer. The increased amount of $Gd(MAA)_3$ enhances the crosslinking of the metallized acrylic and raises the bending strength. Oppositely, increased $Gd(MAA)_3$ weakens the impact strength, which makes this material become fragile. Ultimately, the content of $Gd(MAA)_3$ was determined to be 5% considering the comprehensive performance. Then, the proportional relation between neutron and X-ray shielding properties and material thickness was analyzed. Moreover, the quasi-static uniaxial tensile stress–stain responses of metallized acrylic containing Gd and Pb under strain rates ranging from 1.67×10^{-4} s^{-1} to 3.33×10^{-3} s^{-1} and temperatures ranging from 60 to 100 °C were studied. It is observed that the viscoelastic tensile responses of the as-prepared metallized acrylic are dependent on strain rate and also temperature. With decline of strain rate or increase of temperature, the modulus of this material obviously decreases. Moreover, the stress–strain responses of this material exhibit hyperelastic and viscoelastic characteristics at the same time. Therefore, the rate and temperature-dependent properties were investigated by fitting the modified ZWT constitutive model, in which the standard elastic component is replaced by the Mooney–Rivlin hyperelastic model, to the experimental test data. The constitutive parameters were determined by nonlinear fitting and interpolated with a function of temperature. The interpolation functions can accurately fit the parameters with temperature change. The great difference in constitutive parameters implies that the viscoelastic response of the as-prepared metallized acrylic affects the apparent behavior to quasi-static tensile loading the most. In conclusion, all results indicate that the constitutive model used herein can accurately describe the tensile nonlinear viscoelastic responses of metallized acrylic containing Gd and Pb under quasi-static loading over a range of strain rate and temperature.

Author Contributions: Conceptualization, B.Z.; methodology, B.Z.; software, F.W.; validation, F.W. and Y.L.; formal analysis, F.W.; investigation, H.Y.; resources, H.Y.; data curation, B.Z.; writing—original draft preparation, B.Z.; writing—review and editing, L.L.; visualization, H.Y.; supervision, L.L.; project administration, Y.Z.; funding acquisition, Y.Z. All authors have read and agreed to the published version of the manuscript.

Funding: This research was funded by Technology and Industry for National Defense, PRC. KZ561936144.

Data Availability Statement: No new data were created or analyzed in this study. Data sharing is not applicable to this article.

Conflicts of Interest: The authors declare no conflict of interest.

References

1. Louis, H.K.; Refeat, R.M.; Hassan, M.I. Control rod shadowing effect in PWR core utilizing Urania-Gadolinia fuel. *Prog. Nucl. Energy* **2021**, *142*, 103993. [CrossRef]
2. Uguru, E.H.; Sapli, M.F.B.A.; Sani, S.A.; Khandaker, M.U.; Rabir, M.H.; Karim, J.A.; Bradley, D.A. Impact of weight percent gadolinium and the number of its fuel rods on the neutronic and safety parameters. *Radiat. Phys. Chem.* **2021**, *188*, 109686. [CrossRef]
3. Tanaka, T.; Hagiwara, K.; Gazzola, E.; Ali, A.; Ou, I.; Sudo, T.; Kumar Das, P.; Singh Reen, M.; Dhir, R.; Koshio, Y. Gamma-ray spectra from thermal neutron capture on gadolinium-155 and natural gadolinium. *Prog. Theor. Exp. Phys.* **2020**, *2020*, 43D02. [CrossRef]
4. Zhang, P.; Jia, C.; Li, J.; Wang, W. Shielding composites for neutron and gamma-radiation with Gd2O3@ W core-shell structured particles. *Mater. Lett.* **2020**, *276*, 128082. [CrossRef]
5. Mahmoud, M.; Makhlouf, S.A.; Alshahrani, B.; Yakout, H.A.; Shaaban, K.S.; Wahab, E.A. Experimental and simulation investigations of mechanical properties and gamma radiation shielding of lithium cadmium gadolinium silicate glasses doped erbium ions. *Silicon* **2022**, *14*, 2905–2919. [CrossRef]

6. Cheewasukhanont, W.; Limkitjaroenporn, P.; Sayyed, M.I.; Kothan, S.; Kim, H.J.; Kaewkhao, J. High density of tungsten gadolinium borate glasses for radiation shielding material: Effect of WO_3 concentration. *Radiat. Phys. Chem.* **2022**, *192*, 109926. [CrossRef]
7. Dong, M.G.; Xue, X.X.; Singh, V.P.; Yang, H.; Li, Z.F.; Sayyed, M.I. Shielding effectiveness of boron-containing ores in Liaoning province of China against gamma rays and thermal neutrons. *Nucl. Sci. Tech.* **2018**, *29*, 58. [CrossRef]
8. Mheemeed, A.; Hasan, H.; Al-Jomaily, F. Gamma-ray absorption using rubber—Lead mixtures as radiation protection shields. *J. Radioanal. Nucl. Chem.* **2012**, *291*, 653–659. [CrossRef]
9. Tisell, L.E.; Hansson, G.; Lindberg, S.; Ragnhult, I. Hyperparathyroidism in persons treated with X-rays for tuberculous cervical adenitis. *Cancer* **1977**, *40*, 846–854. [CrossRef]
10. Griffith, J.A.; Bayer, T.S. A bio-inspired chemical sensor of gamma and neutron radiation. *Sens. Actuators B* **2014**, *190*, 818–821. [CrossRef]
11. Lin, Q.; Yang, B.; Li, J.; Meng, X.S.; Shen, J.C. Synthesis, characterization and property studies of Pb^{2+}-containing optical resins. *Polymer* **2000**, *41*, 8305–8309. [CrossRef]
12. Chen, J.B.; Jiang, P.P.; Lin, X.M. Study on Preparation and Performance of Organic Glass Containing Pb by Microemulsion Polymerization. *China Plast. Ind.* **2008**, *02*, 67–70.
13. Fu, Q.; Bu, M.X.; Xu, W.R.; Chen, L.; Li, D.; He, J.Q.; Kou, H.L.; Li, H. Comparative analysis of dynamic constitutive response of hybrid fibre-reinforced concrete with different matrix strengths. *Int. J. Impact Eng.* **2021**, *148*, 103763. [CrossRef]
14. Liu, Q.; Chen, P.W.; Zhang, Y.; Li, Z.R. Compressive behavior and constitutive model of polyurea at high strain rates and high temperatures. *Mater. Today Commun.* **2020**, *22*, 100834. [CrossRef]
15. Xiao, Y.C.; Fan, C.Y.; Wang, Z.J.; Sun, Y. Visco-hyperelastic constitutive modeling of the dynamic mechanical behavior of HTPB casting explosive and its polymer binder. *Acta Mech.* **2020**, *231*, 2257–2272. [CrossRef]
16. Qiao, Y.; Wang, P.F.; Xue, X.; Liu, M.; Xu, S.L. Enhancing the dynamic temperature stability of epoxy with graphene oxide. *Mech. Mater.* **2020**, *150*, 103593. [CrossRef]
17. Balandin, V.V.; Selyutina, N.S.; Petrov, Y.V. Effect of the Mass Fraction of Ice on the Strain Rate Dependence of Strength under Dynamic Fracture of Frozen Soil. *J. Appl. Mech. Tech. Phys.* **2019**, *60*, 533–538. [CrossRef]
18. Wang, J.; Xu, Y.J.; Zhang, W.H. Finite element simulation of PMMA aircraft windshield against bird strike by using a rate and temperature dependent nonlinear viscoelastic constitutive model. *Compos. Struct.* **2014**, *108*, 21–30. [CrossRef]
19. Dar, U.A.; Zhang, W.H.; Xu, Y.J. Numerical implementation of strain rate dependent thermo viscoelastic constitutive relation to simulate the mechanical behavior of PMMA. *Int. J. Mech. Mater. Des.* **2014**, *10*, 93–107. [CrossRef]
20. Zhang, H.; Wang, L.; Zheng, K.; Bakura, T.J.; Totakhil, P.G. Research on compressive impact dynamic behavior and constitutive model of polypropylene fiber reinforced concrete. *Constr. Build. Mater.* **2018**, *187*, 584–595. [CrossRef]
21. Fu, T.T.; Zhu, Z.W.; Zhang, D.; Liu, Z.J.; Xie, Q.J. Research on damage viscoelastic dynamic constitutive model of frozen soil. *Cold Reg. Sci. Technol.* **2019**, *160*, 209–221. [CrossRef]
22. Zhu, J.; Hu, S.; Wang, L. An analysis of stress uniformity for concrete-like specimens during SHPB tests. *Int. J. Impact Eng.* **2009**, *36*, 61–72. [CrossRef]
23. Wang, L.L.; Yang, L.M. *The Progress in Impact Dynamics*, 1st ed.; The Press of Chinese Sciences and Technology University: Hefei, China, 1992; pp. 88–116.
24. Xu, X.; Gao, S.Q.; Zhang, D.M.; Niu, S.H.; Jin, L.; Ou, Z.C. Mechanical behavior of liquid nitrile rubber-modified epoxy resin: Experiments, constitutive model and application. *Int. J. Mech. Sci.* **2019**, *151*, 46–60. [CrossRef]
25. Jiang, J.; Xu, J.S.; Zhang, Z.S.; Chen, X. Rate-dependent compressive behavior of EPDM insulation: Experimental and constitutive analysis. *Mech. Mater.* **2016**, *96*, 30–38. [CrossRef]
26. Wang, C.; Wang, S.; Zhang, Y.; Wang, Z.; Liu, J.; Zhang, M. Self-polymerization and co-polymerization kinetics of gadolinium methacrylate. *J. Rare Earths* **2018**, *36*, 298–303. [CrossRef]
27. Zhang, Y.J.; Guo, X.T.; Wang, C.H.; Lu, X.A.; Wu, D.F.; Zhang, M. Gadolinium-and lead-containing functional terpolymers for low energy X-ray protection. *Nucl. Eng. Technol.* **2021**, *53*, 4130–4136. [CrossRef]
28. Hui, H. Study on the Metal-Containing Optical Plastics. Master's Thesis, Changchun University of Science and Technology, Changchun, China, 2000.
29. Zhang, Y.J.; Wang, C.H.; Wu, D.F.; Guo, X.T.; Yu, L.; Zhang, M. Probing the effect of straight chain fatty acids on the properties of lead-containing plexiglass. *React. Chem. Eng.* **2021**, *6*, 1628–1634. [CrossRef]
30. Wang, C.R.; Wang, C.H.; He, M.M.; Li, T.; Yan, C.H.; Zhang, M. Preparation and Properties of Gd3+-Containing Organic Glass. *Rare Met.* **2010**, *34*, 568–573.
31. Liming, Y.; Lilih, W.; Zhaoxiang, Z. A micromechanical analysis of the nonlinear elastic and viscoelastic constitutive relation of a polymer filled with rigid particles. *Acta Mech. Sin.* **1994**, *10*, 176–185. [CrossRef]
32. Hoss, L.; Marczak, R.J. Hyperelastic Constitutive Models for Incompressible Elastomers: Fitting, Performance Comparison and Proposal of a New Model. In Proceedings of the 20th International Congress of Mechanical Engineering, Gramado, Brazil, 15–20 November 2009.
33. Steinmann, P.; Hossain, M.; Possart, G. Hyperelastic models for rubber-like materials: Consistent tangent operators and suitability for Treloar's data. *Arch. Appl. Mech.* **2012**, *82*, 1183–1217. [CrossRef]

34. Khajehsaeid, H.; Arghavani, J.; Naghdabadi, R. A hyperelastic constitutive model for rubber-like materials. *Eur. J. Mech. -A/Solids* **2013**, *38*, 144–151. [CrossRef]
35. Koziey, B.; Ghafur, M.; Vlachopoulos, J.; Mirza, F. Computer simulation of thermoforming. In *Composite Sheet Forming*; Composite Materials Series; Elsevier: Amsterdam, The Netherlands, 1997; pp. 75–89.
36. Bourgin, P.; Cormeau, I.; Saint-Matin, T. A first step towards the modelling of the thermoforming of plastic sheets. *J. Mater. Processing Technol.* **1995**, *54*, 1–11. [CrossRef]
37. Nam, G.J.; Lee, J.W.; Ahn, K.H. Three-dimensional simulation of thermoforming process and its comparison with experiments. *Polym. Eng. Sci.* **2000**, *40*, 2232–2240. [CrossRef]
38. Destrade, M.; Saccomandi, G. Finite-amplitude inhomogeneous waves in Mooney–Rivlin viscoelastic solids. *Wave Motion* **2004**, *40*, 251–262. [CrossRef]